When is template directed mineralization really template directed?

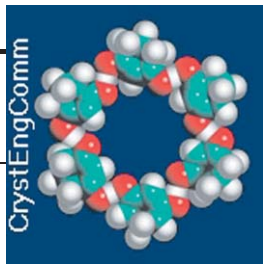

Communication

Elaine DiMasi,*[a] Matthew J. Olszta,[b] Vishal M. Patel[b,c] and Laurie B. Gower[b]

[a]*Physics Department, Brookhaven National Laboratory, Upton, NY, 11973, USA. E-mail: dimasi@bnl.gov; Fax: +1 631-344-2211; Tel: +1 631-344-2739*
[b]*Department of Materials Science and Engineering, University of Florida, Gainesville, FL, 32610, USA*
[c]*College of Medicine, University of Florida, Gainesville, FL, 32611, USA*

Received 14th August 2003, Accepted 10th September 2003
First published as an Advance Article on the web 19th September 2003

***In-situ* synchrotron X-ray scattering clarifies the role of templating on calcium carbonate mineralization. Fatty acid monolayers are reorganized by Ca^{2+} in the subphase, into structures with no epitaxial relation to $CaCO_3$ planes. Crystals are not oriented relative to the film; kinetics dominates polytype selection.**

Biomineralization is a process by which living organisms produce hard tissues with exceptional physical properties, by virtue of finely controlled microstructure, morphology, and hierarchical organization of the minerals and accompanying organic material. In pursuit of comparable synthetic materials, the processes by which minerals nucleate from solution in the presence of organic species have been under intense study in recent years, because it is clear that the organic matter controls and defines the end product in biogenic mineralization.

Open questions remain concerning both the insoluble organic matrix and soluble entities such as the acidic proteins commonly associated with biominerals. Many mechanisms for control of mineralization are proposed: macromolecules may provide boundaries for compartmentalization of ions prior to nucleation, or charged surfaces which locally change the solution composition. An ordered insoluble organic template may direct crystallization *via* stereochemical alignment between functional groups or by epitaxial atomic-scale registry between charge positions in the organic and mineral structures; or, a protein may recognize and bind to specific crystal faces, affecting growth and morphology. More recently, it has been proposed that the acidic proteins may act as process-directing agents, in which the solution crystallization is transformed into a precursor process.[1] It is hoped that simplified experiments with well defined mineral or organic surfaces will allow these competing mechanisms to be distinguished, but many experiments suffer from a lack of *in-situ* structural information.

A significant number of publications have described mineralization of calcium carbonates from solution against self-assembled films of amphiphilic molecules, either on solid substrates[2] or at liquid surfaces.[3–9] Observations of macroscopic crystal morphology or orientation relative to the organic are suggestive of epitaxial templating in many of these studies. At the same time, it has been remarked repeatedly that functionalized organic surfaces can influence both structural and kinetic aspects of mineral phase formation.[10–13] Furthermore, the ion concentrations, temperature, and pH are known to affect the structures of such surfactant assemblies.[14–16] For these reasons it is crucial to monitor the structures of both template and mineral during nucleation, to correctly distinguish kinetic from epitaxial or stereochemical control. Only recently have *in-situ* methods such as synchrotron X-ray scattering and neutron reflectivity been applied to mineralizing

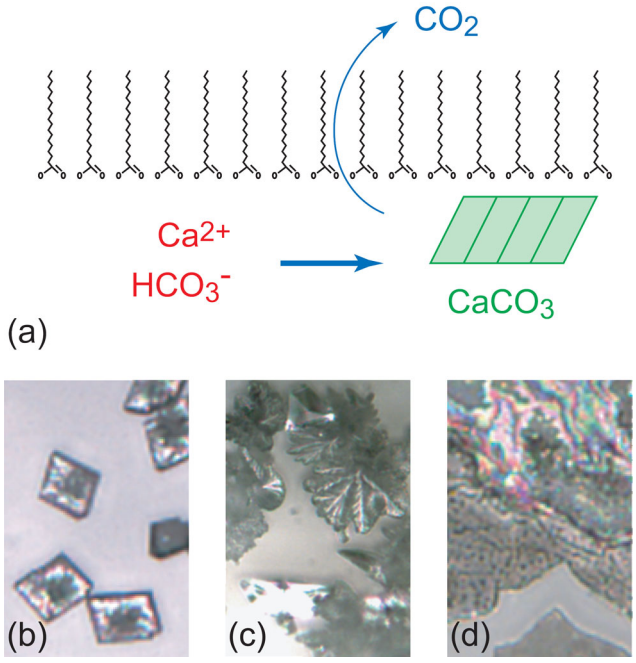

Fig. 1 (a) Depiction of fatty acid template on the supersaturated calcium bicarbonate solution. CO_2 escape precipitates calcium carbonate, which nucleates preferentially at the monolayer. (b) Rhombohedral calcite favored during fast mineralization. (c) Vaterite florets obtained from rate-inhibited mineralization. (d) Birefringent calcite thin film grown through an amorphous precursor phase by the addition of poly(acrylic acid, sodium salt), 32 μg ml^{-1}, MW 8000. Height of optical micrograph panels (b)–(d) is 200 μm.

film systems.[17–20] No report so far has presented direct structural evidence for epitaxy in calcium carbonates.

Here we describe surface-sensitive synchrotron X-ray scattering from Langmuir monolayers of fatty acids assembled on a supersaturated calcium bicarbonate subphase (Fig. 1a). Escape of carbon dioxide gas precipitates $CaCO_3$, and in the absence of a monolayer film, the thermodynamically stable calcite polymorph is obtained in the form of rhomb-shaped crystals. A series of influential papers published fifteen years ago[3–6] showed that $CaCO_3$ nucleating at surfactant monolayers can crystallize as flattened calcite rhombs (Fig. 1b) or polycrystalline "florets" of the less stable vaterite polytype (Fig. 1c). In the above-mentioned studies the authors made two essential points: (i) vaterite could be induced by a stearic acid monolayer, dependent upon the surface pressure of the film; (ii) macroscopic vaterite crystals observed by optical microscopy or harvested for electron diffraction appeared to be oriented with the *c*-axis normal to the monolayer plane. The authors concluded from these observations that a stereochemical match

 DOI: 10.1039/b309800a

between the orientations of the charged fatty acid headgroups and the carbonate groups in vaterite, combined with favorable cation positions in vaterite as opposed to calcite, promoted vaterite formation at the surface. The original study worded these findings cautiously and provided very thorough characterizations of the system. But in its wake, the importance of a stereochemical or even epitaxial template is now sometimes taken for granted.

In-situ X-ray scattering measurements demonstrate instead that the $CaCO_3$ polytype is determined primarily by kinetic effects and does not depend explicitly upon the structure of the monolayer film. Our experiments reproduce the results of the previous studies[3–6] of $CaCO_3$ nucleation under stearic acid monolayers under similar conditions of subphase concentration, surface pressure, and pH. However, we interpret most of these results in a new light, based on the structural information obtained from the X-ray experiments, as well as from new experiments with slight but significant changes to the experimental conditions: changes to the CO_2 gas diffusion rate, hydrocarbon chain length, and supersaturation. For comparison, we will also discuss polycrystalline calcite films (Fig. 1d), which form through a metastable amorphous precursor phase by the addition of poly(acrylic acid) to the subphase.[20,21] The amorphous precursor films nucleate slowly enough to enable time-dependent measurements of film density and thickness, giving us direct access to kinetic parameters in the clear absence of an epitaxial contribution.

The following experimental methods were employed. Stearic and arachidic acid (sodium salts, purchased from Sigma) were spread onto the subphase as 1 mg ml^{-1} solutions in chloroform using a microliter syringe. The supersaturated calcium bicarbonate subphase was prepared by dissolving $CaCO_3$ powder into pure water by bubbled CO_2 gas. The $CaCO_3$ concentration in solution calculated from weights of the dry filter cakes was $\approx$9 mmol. Filtered solutions, either at full strength or diluted 1 : 1 with pure water, were poured into a Langmuir trough equipped with a computer controlled barrier, a Wilhelmy balance made from filter paper and calibrated by a hanging weight, and an enclosed environment to maintain a bath temperature of 19 °C and a flowing helium atmosphere to reduce X-ray background scattering. X-ray measurements were performed at beamline X22B of the National Synchrotron Light Source at a wavelength 1.56 Å. Reflectivity measurements utilized a Bicron scintillator detector with 2 mm slit collimation. Background scattering was subtracted by acquiring counts with the detector displaced from the reflection plane. The best fit model electron density profiles $\rho(z)$ were analyzed in the kinetic limit where $R(q_z)/R_F \propto |\int (\partial\rho/\partial z) \exp(iq_z z)\, dz|^2$, as has been described previously.[20] In-plane scattering measurements were made at incident angle α = 0.12–0.14°. Either a 2D MARCCD detector or a linear position sensitive detector with 10° vertical acceptance was used to resolve intensity in the reflection angle β, while the in-plane scattering angle was resolved in the latter case using a Soller collimator with an 0.2° acceptance.

The simplest question one can address with *in-situ* X-ray scattering is whether the crystals at the surface are crystallographically oriented relative to the monolayer (Fig. 2a). In the case of stearic acid monolayers nucleating the {001} face of vaterite, the diffraction pattern would show (*hk*0) Bragg spots in the monolayer plane at early times, and also at late times if no crystal reorientation took place as they grew. Instead, we always observe a distribution of orientations of vaterite crystals. Figs. 2b and 2c show diffraction patterns obtained several hours after preparation of the sample, using a two-dimensional detector at wide angle within the monolayer plane, which can access a broad range of in-plane scattering angles (marked on the horizontal axis) as well as a 6° vertical component of the scattering angle. The arcs indicate that crystal orientations at the surface are distributed through

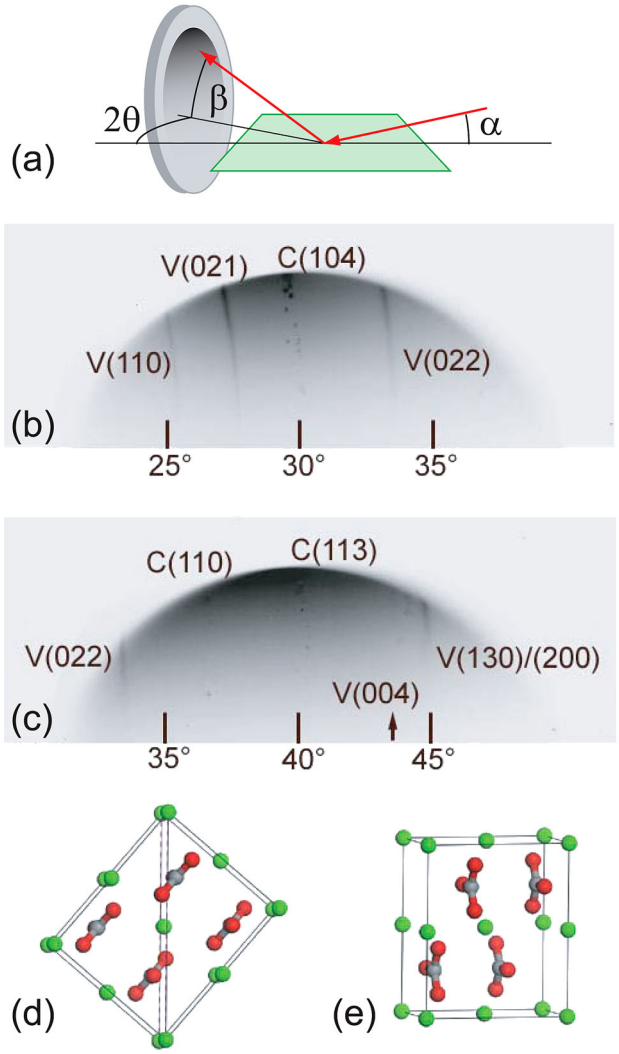

Fig. 2 (a) Grazing incidence diffraction geometry: incident angle α, reflection angle β, in-plane scattering angle 2θ. The C18 monolayer mineralized in air at fixed area on the subphase. The MAR CCD detector at scattering angles of (b) 30° and (c) 40° accesses a range of vaterite (V) and calcite (C) peaks, spanning 16° in 2θ and 6° in β. An almost complete spectrum of vaterite rings is observed (lacking the (004) : arrow in (c)). Discrete calcite peaks indicate a small number of large, individual calcite crystals along with vaterite powder. (d) Vaterite orientation indicated by (022) peaks. (e) Vaterite orientation in the stereochemical model.

angles of at least ±12° about the surface normal. The q dependences of these streaks are distinct from those of Bragg rods which are produced by the organic surface films. The vaterite (021) and (022) rings indicate that a sizable population of crystals are oriented with these planes normal to the surface plane, *i.e.*, as shown in Fig. 2d. These orientations are present together with the "stereochemically templated" orientation having the *c*-axis strictly normal to the surface, the model depicted in Fig. 2e. In all of our experiments, performed *in-situ* without disturbing the Langmuir trough, the earliest detectable Bragg peaks (usually the (022), (021) and (110) together in the same spectra) always show the orientational distributions indicative of random powders, consistent with the complete ring spectra observable at later times when a greater volume of scatterers has accumulated at the surface.[22] These data argue strongly against the model of oriented vaterite, and against the mechanism of stereochemical alignment of carbonate, which would not favor tilts such as that in Fig. 2d. The strongest peaks from the vaterite spectrum which are missing from our observed angular range are the (113) and (004). It is already recognized that once a crystal achieves a large size and

anisotropic shape, surface tension effects may reorient it.[13] Probably such effects in the case of the vaterite florets reorient the largest crystals such that high L-index peaks are not found within $\pm 12^{\circ}$ of the surface normal. Macroscopic reorientation certainly plays some role for the large crystals observed by optical microscopy, and probably for those harvested onto grids for electron microscopy,[13] the methods used in the past to assess crystal orientation.

Calcite reflections are also evident in our diffraction patterns, even for experiments which nucleate predominantly vaterite. Clearly, these two phases compete at the surface. To understand the factors that control $CaCO_3$ formation at the monolayer, we must use the X-ray measurements to scrutinize other aspects of the surface structure, including the in-plane structure of the monolayer and the quantity of cations bound to the monolayer.

Cation binding at the COOH headgroups is a function of their degree of deprotonation, depending upon the solution pH relative to the fatty acid dissociation constant pK_a. In our supersaturated calcium bicarbonate solutions which mineralize over time, the pH rises from 6.3 to about 7.4 in a few hours.[23] Under these conditions we estimate that the headgroups are no more than 50% deprotonated,[24,25] and we do not expect to observe the formation of a stoichiometric Stern layer of Ca^{2+} ions. Nevertheless, any quantity of cations bound to the monolayer will change the charge and concentration gradients in that region, and affect the relative stability of the mineral polytypes. We have determined the cation binding quantitatively from X-ray reflectivity measurements, in which the interference pattern from electron density modulations along the surface normal is measured and interpreted in terms of a model surface-normal profile.[20] Fig. 3a shows reflectivity curves from stearic acid monolayers compressed on water (○) and on the calcium bicarbonate subphase (Δ). Increased intensity and amplitude of oscillations in the latter data indicate the greater electron density at the headgroup position, shown by models in Fig. 3b. By assigning the additional electron density to a mixture of calcium ions and water molecules, we find there are from 4–8 fatty acid molecules per cation at the surface: not the 2 : 1 or 1 : 1 ratios expected for bidentate or epitaxial adsorption. We previously reported a similar range of cation binding for an arachidic acid film on a calcium bicarbonate solution that had been diluted 1 : 1 with pure water, leading to slightly greater pH of 7.5–8.5 and to a factor of two decrease in Ca concentration in solution.[26,27] Evidently, the degree of deprotonation is approximately the same, and the Ca concentration is sufficient to populate the monolayer to the same extent, in the dilute and full-strength subphases.

Complementary information is obtained from grazing-incidence X-ray diffraction, in which the beam impinges on the surface within the critical angle for total external reflection, illuminating just the surface layers. At early times, before the surface is disrupted by macroscopic crystals, the measurements detect the in-plane order of the surfactant molecules. This technique has already shown that cations in the subphase affect these self-assembled films.[15,16] In the case of stearic and arachidic acids (referred to in the following as C18 and C20, respectively, indicating the length of the hydrocarbon chains), monolayers assembled at high pressure (*ca.* 25 mN m^{-1}) on water are compressed into hexagonal phases, evident from the single Bragg peak (Fig. 4, circles). From the measured lattice parameter a the average molecular area A is known precisely: a = 4.71 and 4.74 Å, A = 19.2 and 19.5 Å^2 per molecule, for C18 and C20 respectively. The headgroup positions in this cell do not closely match the cation positions in the a–b plane of the vaterite cell (a = 4.13 Å, b = 7.15 Å, 14.76 Å^2 per cation: Fig. 4, scheme at top left).

On the calcium bicarbonate subphase, cations at the headgroups change the molecular interactions and stabilize a

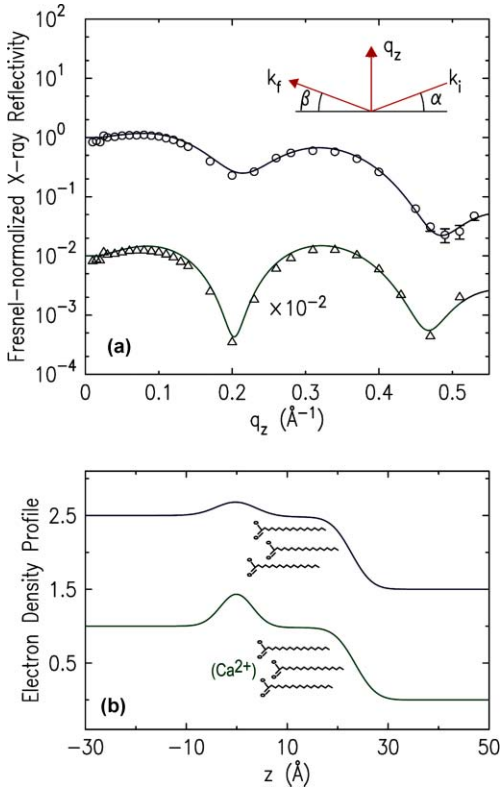

Fig. 3 (a) Fresnel-normalized X-ray reflectivity $R(q_z)/R_F$ from C18 monolayers on water (○) and calcium bicarbonate solution (Δ) at surface pressures of 20–25 mN m^{-1}. Lines are calculated from models in (b). Inset: reflection geometry. (b) Surface-normal electron density profiles $\rho(z)$, normalized to the density of the water subphase. Upper curve: best fit to data on water. Lower curve: calcium bicarbonate subphase. Schemes show the positions of molecules at the surface. Increased density in the headgroup region, modeled by a Gaussian, shows that calcium collects at the interface of the bicarbonate subphase. The Ca^{2+} binding was computed by subtracting the Gaussian contribution from the water measurement, and assuming that excess electrons come from a combination of Ca^{2+} and H_2O. Taking the volume ratios of these two species in the range 0.4–1.0 we estimate 4–8 molecules per cation.

closely-packed rectangular unit cell, as indicated by the two peaks in the diffraction pattern (Fig. 4, triangles).[26] The rectangular cell parameters for the C18 and C20 films are a = 4.91, 4.93 ± 0.05 Å; b = 7.66, 7.57 ± 0.05 Å; A = 18.8, 18.7 Å^2 molecule^{-1}. These are *smaller* molecular spacings than for films on water, in contrast to the previous report,[13] which estimated an increased molecular area from a pressure-area isotherm and attributed this increase to the area occupied by cations. The discrepancy between the two reports is due to the fact that our X-ray study accesses the lattice constant directly, and is not affected by the presence of extra space between ordered surfactant domains, or by the nonequilibrium effects of compression. We compared this structure to further experiments on uncompressed films and found that *the lattice is unchanged by the application of surface pressure*. This means that in the presence of the cations, there is no *structural* distinction between "liquid expanded" and "fully compressed" phases: the cations cause the surfactant to self-assemble into close-packed domains even at low surface pressure, and increased pressure simply pushes the ordered regions closer together.

Diffraction patterns from the mineralizing surfaces also allow us to monitor crystallization as it occurs. The diffraction data shown by triangles in Fig. 4 include points which lie far away from the fit curves (marked by arrows): these are calcite (104) reflections. To explain the presence of both calcite and vaterite in our experiments, we must address the carbon dioxide

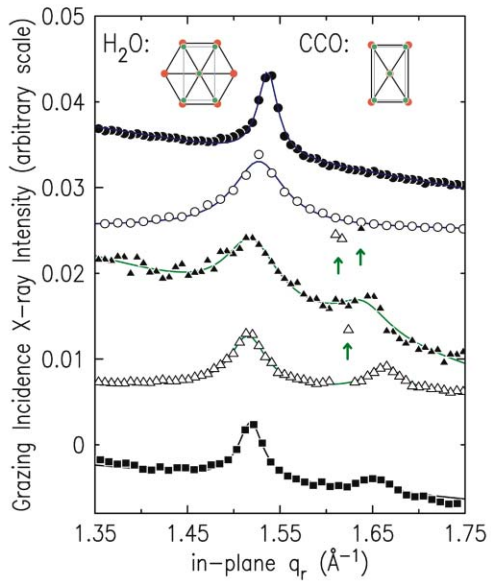

Fig. 4 Grazing incidence diffraction scans. Bragg peaks arise from the molecules at the surface, which organize into domains of order 60 Å. On water, C18 and C20 have hexagonal unit cells at $P \approx 25$ mN m^{-1} (● and ○). On the supersaturated calcium bicarbonate subphase rectangular unit cells are observed (▲: C18, △: C20). The rectangular phase is also observed on a calcium bicarbonate subphase diluted 1 : 1 with pure water (square). Schemes at top compare the hexagonal and rectangular lattice positions of the headgroups (red circles) to the Ca positions in the vaterite *a–b* plane (smaller green circles). Lines are Lorentzian fits. In the rectangular lattice, the peak amplitudes have a 2 : 1 ratio allowing them to be indexed as the (11) and (02) peaks. On the dilute subphase, the peak ratio is 5 : 1, likely an indication that the film was nonuniform. Arrows indicate positions of calcite (104) reflections (shifted in q_r due to the projection of the data onto the q_r axis over the range of β).

gas escape that drives mineralization. In many $CaCO_3$ mineralization studies that we are aware of, gas diffusion is controlled poorly if at all. In the case of our X-ray experiments, we found significant differences in phase formation that could be attributed to the aspect ratio of the sample trough. Specifically, in order to be sensitive to the weak signal from the monolayer structure, we utilized a large sample area of 12 cm along the beam direction and several cm in the transverse direction. The water depth was restricted to a few mm, to avoid disruptive surface waves. The large surface to volume ratio of this configuration leads to rapid gas escape, as does the reduced CO_2 overpressure (relative to air) in the flowed helium gas environment of the synchrotron apparatus. Although vaterite mineralization occurred, calcite formation was significantly favored in this shallow trough.

To grow a full coverage of vaterite as the previous publications reported, a cell with 1 × 2 cm^2 surface area and 10 mm depth was used and allowed to crystallize in air. Additional experiments confirmed that the in-plane film structure does not depend on the atmosphere. The scattering volume in this case is insufficient to study the monolayer structure, but allows characterization of the final product as we showed in Fig. 2. We can conclude that *the first significant contributor to the kinetics is the rate of CO_2 gas escape, which can select vaterite versus calcite against an identical fatty acid structure*. This result is consonant with a recent report that finds that variations in fatty acid chain length affect the induction time, mineralization rate, and proportions of vaterite to calcite nucleated at Langmuir films, because of the difference in CO_2 diffusion through the thicker films of long-chain surfactants.[13]

We also examined the effects of reducing calcium concentration, reported previously to select vaterite over calcite,[5] by diluting the supersaturated subphase 1 : 1 with pure water. This change in supersaturation turns out to have essentially no effect on either the monolayer structure (Fig. 4, squares), or the cation binding determined from reflectivity.[26] Vaterite crystals are obtained in large quantity even for the shallow sample trough geometry. This is a curious finding since generally the metastable phases are favored under conditions of higher supersaturation. We believe that the explanation lies in the changes in the stoichiometric balance between bound and mobile cations, and carbonate species produced in the vicinity of the monolayer. In this context, it is interesting to consider the effects of inhibitors such as poly(acrylic acid) (PAA) in solution, which can favor the formation of less stable phases. We and others have explored the formation of amorphous calcium carbonate precursor films in the presence of polymers[20,21] (Fig. 1d). The polymer slows mineralization enough to enable us to measure film thicknesses from 3 to 30 nm over the course of 10–30 h using X-ray reflectivity.[20] In our measurements of C20 films with PAA in 10–100 μg ml^{-1} quantities (molecular weight 5000–8000), the cation binding is reduced to 15–25 molecules per cation, suggesting that the polymer removes Ca^{2+} from solution and thus from the monolayer. This charge redistribution acts along with the CO_2 escape in governing mineralization. Gas escape is rate limiting for thin trough geometries: films grow in thickness at a rate independent of polymer concentration. Adding more polymer increases the lifetime of the metastable amorphous film, but cannot prevent the subsequent dissolution. Reduction of gas escape rate (deep trough) causes film deposition to occur more slowly, but improves the stability of the amorphous phase and enables the film to crystallize as calcite. A complete report of polymer-induced amorphous precursor formation at Langmuir films is underway by our group.

In summary, we have presented surface X-ray scattering measurements of calcium carbonates nucleating from solution against fatty acid monolayers. These measurements provide new information to address the concepts of epitaxial control which are prevalent in the biomimetics literature. In contrast to earlier reports using similar conditions, we found that vaterite crystals nucleated by stearic and arachidic acid films are not oriented relative to the monolayer. X-ray reflectivity measurements of the cation binding find values of 4–8 molecules per Ca^{2+} at the monolayer: a result not suggestive of an epitaxial mechanism for promoting the vaterite polytype. Grazing-incidence diffraction from monolayers under a variety of solution conditions finds that a rectangular unit cell forms in the presence of these cations, essentially independent of applied surface pressure, solution supersaturation, or CO_2 overpressure. The template-independent variations in solution kinetics can select vaterite over calcite, the former being favored when mineralization occurs more slowly due to a change of stoichiometry of reactants near the monolayer. In all experiments, the dominant factor in polymorph selectivity was found to be the CO_2 escape rate. The *in-situ* structural information obtained in our experiments has allowed us to make very specific statements about kinetic *vs.* stereochemical or epitaxial mechanisms in this system for the first time. Synchrotron X-ray scattering techniques will play an important part in future studies of organic-mediated and structurally templated mineralization.

Acknowledgements

The National Synchrotron Light Source is supported under USDOE contract DE-AC02-98CH10886. The authors acknowledge BNL LDRD 02-67, the Particle Engineering Research Center (PERC) at UF, the NSF (EEC-94-02989 and DMR-0094209), and Industrial Partners of the PERC for support of this research.

References

1 L. B. Gower and D. J. Odom, *J. Cryst. Growth*, 2000, **210**, 719.
2 J. Aizenberg, A. J. Black and G. M. Whitesides, *J. Am. Chem. Soc.*, 1999, **121**, 4500.
3 S. Mann, B. R. Heywood, S. Rajam and J. D. Birchall, *Nature (London)*, 1988, **334**, 692.
4 S. Mann, B. R. Heywood, S. Rajam and J. D. Birchall, *Proc. R. Soc. London*, 1989, **A423**, 457.
5 S. Rajam, B. R. Heywood, J. B. A. Walker and S. Mann, *J. Chem. Soc., Faraday Trans.*, 1991, **87**, 727.
6 B. R. Heywood, S. Rajam and S. Mann, *J. Chem. Soc., Faraday Trans.*, 1991, **87**, 735.
7 J. Lahiri, G. Xu, D. M. Dabbs, N. Yao, I. A. Aksay and J. T. Groves, *J. Am. Chem. Soc.*, 1997, **119**, 5449.
8 P. J. J. A. Buijnsters, J. J. J. M. Donners, S. J. Hill, B. R. Heywood, R. J. M. Nolte, B. Zwanenburg and N. A. J. M. Sommerdijk, *Langmuir*, 2001, **17**, 3623.
9 D. Volkmer, M. Fricke, C. Agena and J. Mattay, *CrystEngComm*, 2002, **4**, 288.
10 L. Addadi and S. Weiner, *Angew. Chem., Int. Ed. Engl.*, 1992, **31**, 153.
11 S. Mann, V. Wade, A. Treffry, S. J. Yewdall, P. M. Harrison, S. Levi and P. Arosio, in *Chemistry and Biology of Mineralized Tissues*, ed. H. Slavkin and P. Price, Elsevier, 1992, pp. 399–408.
12 K. Naka and Y. Chujo, *Chem. Mater.*, 2001, **13**, 3245.
13 E. Loste, E. Díaz-Martí, A. Zarbakhsh and F. C. Meldrum, *Langmuir*, 2003, **19**, 2830.
14 A. Firouzi, D. Kumar, L. M. Bull, T. Besier, P. Sieger, Q. Huo, S. A. Walker, J. A. Zasadzinski, C. Glinka, J. Nicol, D. Margolese, G. D. Stucky and B. F. Chmelka, *Science (Washington, D. C.)*, 1995, **267**, 1138.
15 V. M. Kaganer, H. Möhwald and P. Dutta, *Rev. Mod. Phys.*, 1999, **71**, 779.
16 J. Kmetko, A. Datta, G. Evmenenko and P. Dutta, *J. Phys. Chem. B*, 2001, **105**, 10818.
17 S. A. Holt, G. J. Foran and J. W. White, *Langmuir*, 1999, **15**, 2540.
18 T. Brennan, A. V. Hughes, S. J. Roser, S. Mann and K. J. Edler, *Langmuir*, 2002, **18**, 9838.
19 J. Kmetko, C. Yu, G. Evmenenko, S. Kewalramani and P. Dutta, *Phys. Rev. Lett.*, 2002, **89**, 186102.
20 E. DiMasi, V. M. Patel, M. Sivakumar, M. J. Olszta, Y. P. Yang and L. B. Gower, *Langmuir*, 2002, **18**, 8902.
21 G. Xu, N. Yao, I. A. Aksay and J. T. Groves, *J. Am. Chem. Soc.*, 1998, **120**, 11977.
22 We are aware of similar measurements by J. Kmetko and P. Dutta on the fatty acid/$CaCO_3$ system, who independently came to the same conclusion (unpublished).
23 This is a higher pH than the 4.5–5.0 range often quoted as the "pK_a of fatty acids" (ref. 3). However, this quote applies to short-chain fatty acids. Increased hydrocarbon tail length increases the pK_a, to values in the range 8–10 for stearic and arachidic acids (refs. 24,25).
24 J. R. Kanicky, A. F. Poniatowski, N. R. Mehta and D. O. Shah, *Langmuir*, 2000, **16**, 172.
25 J. R. Kanicky and D. O. Shah, *J. Colloid Interface Sci.*, 2002, **256**, 201.
26 E. DiMasi and L. B. Gower, *Mat. Res. Soc. Symp. Proc.*, 2002, **711**, 301.
27 This preliminary report of hexagonal structure for arachidic acid on the diluted calcium carbonate subphase was erroneous, due to beam damage of the film. Subsequent measurements monitoring the oxygen partial pressure in the trough confirmed the reflectivity results, and the rectangular structure reported in the present work.